Molecular Modeling of Small-Molecule Permeation in Polyimides and Its Correlation to Free-Volume Distributions

Matthias Heuchel,*,† Dieter Hofmann,† and Pluton Pullumbi‡

GKSS Research Center, Institute of Chemistry, Kantstr. 55, D-14513 Teltow, Germany, and Air Liquide, Centre de Recherche Claude Delorme, Les Loges-en-Josas, B.P. 126, 78350 Jouy-en-Josas, France

Received September 12, 2003; Revised Manuscript Received November 5, 2003

ABSTRACT: Well-equilibrated molecular-packing models have been produced for 10 different polyimides. The Gusev−Suter transition-state theory was used to calculate gas solubilities and diffusion coefficients for nitrogen, oxygen, methane, and carbon dioxide. Good agreement with experiment (factors 1−4) was found, except for CO_2. The difficulties in this comparison were discussed. A significant improvement from former results could be assessed for the predicted O_2/N_2 selectivity values. The simulated models allow an accurate determination of structural parameters, either as a single parameter, like the fractional free volume, or as size-distribution function of free-volume elements accessible for a certain penetrant. The 2,2′-bis(3,4-dicarboxy-phenyl) hexafluoropropane polyimides with the highest oxygen permeability (50−130 Barrer) show a wider size distribution with an additional peak or shoulder at larger radii (>5−6 Å) than conventional polyimides. A constitutive structural element seems to be the *o*-methyl groups in the aromatic diamine moiety.

1. Introduction

1.1. Polyimides in Gas Separation. Polyimides (PIs) have attracted much attention over the last years as material for gas-separation membranes.[1−3] Particular polyimides synthesized from 2,2′-bis(3,4-dicarboxy-phenyl) hexafluoropropane dianhydride (6FDA) show surprisingly high gas selectivities for gas pairs such as O_2/N_2 and CO_2/CH_4. Combined with high inherent chemical and thermal stability as well as mechanical strength, these polyimides have been identified as promising materials for applications such as the recovery of H_2 from industrial gas mixtures of CO_2, N_2, or CH_4; the purification of natural gas; and the enrichment of either O_2 or N_2 from air.

One stimulus for the extensive research was the observed tradeoff relationship between gas permeability and permselectivity. Over the last two decades, intensive investigations have been done to study the structure−property relationships of polyimides by systematically changing the diamine or dianhydride moieties.[4−6] Analysis of this immense experimental material allowed the development of empirical principles. It was found that the incorporation of bulky groups into the polymer backbone increased the permeability, whereas rigid polymeric segments tended to enhance the permselectivity. A good example is the hexafluoropropane $-C(CF_3)_2-$ linkage in 6FDA-based polyimides, which hinders the rotation of neighboring phenyl rings. As a result, the respective polyimides show higher selectivity values at a specific permeability than polyimides without this group.[7,8]

The indications of the last paragraph concerning the possible connection between polymer structure and the transport properties of permeating gases in these structures show already the complexity of this relation. Therefore, it is highly desirable to investigate these systems also on an atomistic level. Over the last years, molecular-modeling investigations have already been used to get a deeper insight in the structure and the transport behavior of nonporous amorphous polymer membranes. General results of these investigations can be found, e.g., in a number of references and feature articles.[9−12]

In this paper, we want to show on 10 polyimides how adequate atomistic packing models can be "built" with molecular-modeling techniques for such glassy, rigid-rod-like polymers. First, we will describe the principal steps for constructing the models. Then, we will test the quality of the packings by calculating solubility and diffusion values for the gases oxygen, nitrogen, methane, and carbon dioxide using a transition-state theory (TST). The results will be compared with experimental data. Then, we will compare the respective selectivity values for O_2/N_2 mixtures with experiments. To understand better the predicted transport values, we will calculate other structural properties such as the distribution of free-volume regions from the developed packing models of the PIs. These structural features will be correlated with the permeability of small molecules.

1.2. Experimental Gas Transport Data for a Comparison with Simulation Data. Most experimental permeation measurements are done with an industrial background, typically at conditions of, e.g., a pressure of $p = 10$ bar and at a temperature of $T = 308$ K. Later in this work, we will have to compare our "theoretically" derived values for gas transport in PIs with such literature data. To evaluate correctly these experimental data, it is useful to review shortly the main quantities for a description of gas transport in polymers and to highlight especially the specific experimental conditions under which these parameters are determined. Detailed information about experimental techniques may be found in the literature.[13,14]

The gas transport through a nonporous polymer layer takes place by a solution diffusion mechanism. The isothermal equilibrium concentration (solubility), *c*, of

* Corresponding author. E-mail: heuchel@gkss.de.
† GKSS Research Center.
‡ Centre de Recherche Claude Delorme.

10.1021/ma035360w CCC: $27.50
Published on Web 12/11/2003

a penetrant gas dissolved in the surface layer of the polymer can be related to pressure p of the penetrant in the adjacent gas phase by the relation

$$c = S(c,p)p \tag{1}$$

where $S(c,p)$ is a solubility coefficient. When the concentration of the penetrant in the polymer is very small, eq 1 reduces to a form of Henry's law and the solubility coefficient $S(c) = S_0 p$. In the case of gas permeation, eq 1 is applied to both opposite sides of a membrane, i.e., for the feed side at $p = p_h$ and at the permeate side for $p = p_l$.

The diffusive transport across the membrane, represented by the flux J, is described by a diffusion coefficient D according to Fick's first law

$$J = -D(c)\frac{dc}{dx} \tag{2}$$

Under *steady-state* conditions (T,$p_h > p_l$ = constant), which establish a constant concentration gradient in the membrane, it follows for the steady-state flow J_s through unit area A of a planar, isotropic, and homogeneous membrane of effective thickness δ from eq 2

$$J_s = \bar{D}(c_h - c_l)/\delta \tag{3}$$

where $\bar{D}$ is the averaged diffusion coefficient over the range of concentration in the membrane, defined by the relation

$$\bar{D} = \int_{c_l}^{c_h} D(c)\, dc/(c_h - c_l) \tag{4}$$

and $D(c)$ is the local diffusion coefficient in the membrane. Further, c_h and c_l are the concentrations at the upstream and downstream sides, respectively. Primarily, the steady-state flux through the membrane is determined in the experiments via the relation

$$J_s = \bar{P}(p_h - p_l)/\delta \tag{5}$$

where $\bar{P}$ is the averaged permeability coefficient or the mean permeability. From eqs 1, 3, and 5, the key relation between averaged transport quantities follows

$$\bar{P} = \bar{D}\bar{S} \tag{6}$$

where $\bar{S}$ stands for the averaged solubility coefficient in the membrane, defined by

$$\bar{S} = \frac{(c_h - c_l)}{(p_h - p_l)} \tag{7}$$

In this equation, c_h and c_l ($<c_h$) are the respective equilibrium concentrations of the penetrant on the opposite sides of the membrane. In experiments, it is often the case that the permeate (or downstream) pressure is negligible, and $\bar{S}$ reduces to $\bar{S} = S_h = c_h/p_h$. This solubility quantity is often measured in a separate (gravimetrical) gas sorption experiment under real *equilibrium conditions*, i.e., at T,p = constant, with long enough measuring times (up to a few days) so that alterations of the polymer matrix with very long relaxation times may have taken place. These relaxations are initiated by the local concentration of the sorbed penetrant molecules. It follows that an averaged diffusion coefficient $\bar{D}$, determined from $\bar{D} = \bar{P}/\bar{S}$ using the measured steady-state quantities $\bar{P}$ and $\bar{S}$, may represent the gas transport in the *quasiequilibrium* of the steady state.

In contrast, for permeation experiments on glassy polymers, the measuring time in the often applied *time-lag* conditions (some minutes up to a few hours) is in general too short for an immediate equilibration of the polymer matrix after uptake of the penetrant molecules. Because of the reduced chain mobility below T_g, one obtains therefore in the experiment only an *apparent* or *effective* diffusion coefficient D_{eff}. This coefficient depends in general on concentration $D_{eff}(c)$ and is usually not independent of the measuring time. The effective permeability coefficient P_{eff} and respective coefficient D_{eff} are determined by recording pressure $p_l(t)$ as a function of time t from the following relations[15]

$$P_{eff} = \frac{V\delta T_0}{ATp_h p_0}\left(\frac{dp_l}{dt}\right)_s \tag{8}$$

$$D_{eff} = \frac{\delta^2}{6\tau} \tag{9}$$

where V is the volume of the downstream measuring chamber, δ is the effective thickness of the membrane, $T_0 = 273.15$ K and $p_0 = 1.013$ bar represent standard conditions, A is the effective membrane surface, T is the measuring temperature, and, as already described, p_h and p_l are the upstream and downstream pressures, respectively. The so-called "*time-lag*" τ is determined by linear regression of the part of the $p_l(t)$ curve where the gradient $(dp_l/dt)_s$ becomes constant as an intercept on the time axis. Both effective values D_{eff} and P_{eff} are often used to determine a solubility value

$$S_{eff} \equiv P_{eff}/D_{eff} \tag{10}$$

It is clear that this solubility value is only an approximation for the "true" averaged solubility $\bar{S}$. One could say that the effective transport quantities P_{eff}, D_{eff}, and S_{eff} are *kinetic* quantities. They depend on the specific conditions in the time-lag experiment. However, P_{eff} will be in general an acceptable measure for $\bar{P} \approx P_{eff}$.

For small concentrations, $D(c)$ merges into a constant diffusion coefficient D_0, and one should observe for decreasing upstream pressures p_h, i.e., at infinitely small dilution, the limiting relation

$$\lim_{c,p\to 0} D(c) = D_0 = \bar{D} = D_{eff} \tag{11}$$

This was recently confirmed by experiment for one of the polyimides (BAAF, see below) studied in this work.[16] Under these limiting conditions, the following relation, similar to eq 6, is valid

$$P_0 = S_0 D_0 \tag{12}$$

where P_0 depends only (despite the temperature) on the nature of the penetrant−polymer system. In fact, just the situation of infinitely small dilution, expressed in eqs 11 and 12, corresponds to the conditions of our later calculations, where we investigate the transport of only a single penetrant molecule through the matrix. Therefore, the "closest" experimental realization of these conditions should be found in permeation experiments performed at very small upstream pressures or for

Scheme 1. Repeat Unit Structure of the Investigated Polyimides

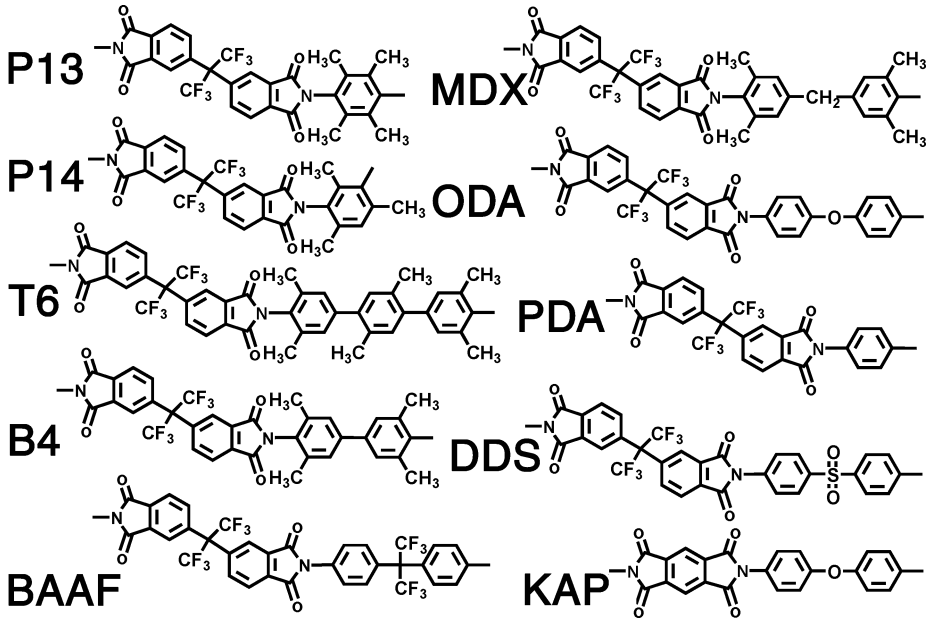

Table 1. Physical Properties of the Polyimides in Scheme 1

PI	name	density (g/cm^3)	T_g (K)	exp P_{O2} (Barrer)
PI3	6FDA-durene	1.32 ± 0.02[59,19,29]	695 ± 3[59,29]	124 ± 45[19,59,29,44,43]
PI4	6FDA-3MPD	1.32 ± 0.03[59,19,62,60,43]	656 ± 8[59,62,60,30]	137 ± 22[59,19,62,60,43]
T6	6FDA-6MTP	1.31[45]	(598)[a]	69[45]
B4	6FDA-TMB	1.30[31]	652 ± 16[31,32]	54[32]
BAAF	6FDA-BAAF 6FDA-6FpDA	1.47 ± 0.01[33,8,34,35,14]	584 ± 11[33,8,34,35,14,16]	13 ± 4[33,8,16]
MDX	6FDA-MDx	1.36 ± 0.0[6,32]	575 ± 50[6,32]	11 ± 10[6,32]
ODA	6FDA-ODA	1.43 ± 0.00[33,8,6,60,36,37,38]	572 ± 11[33,8,6,60,36,37,38]	4 ± 1[33,8,6,60,36,37,38]
PDA	6FDA-PDA	1.47 ± 0.01[59,37,36,35,29]	610 ± 19[59,37,36,35,29]	5 ± 3[59,36,37]
DDS	6FDA-DDS	1.47 ± 0.01[39,40]	604 ± 8[39,40]	3 ± 1[39,40,41]
KAP	PMDA-ODA	1.40 ± 0.01[8,6,7,37,38]	673 ± 1[8,6,38]	0.5 ± 0.3[8,6,7,37,38]

[a] Calculated with Synthia program.

respective extrapolations to $p_h = 0$ (see ref 13), and any directly determined equilibrium solubility in the Henry region should be more trustworthy for a comparison with simulations than effective solubility values, determined *indirectly* from the time-lag experiment after eq 10.

The ideal gas selectivity of a polymer membrane $\alpha^{id}_{A/B}$ is defined by the relation

$$\alpha^{id}_{A/B} \equiv \frac{\bar{P}_A}{\bar{P}_B} = \left(\frac{\bar{D}_A}{\bar{D}_B}\right)\left(\frac{\bar{S}_A}{\bar{S}_B}\right) \qquad (13)$$

where the ratios a $\alpha^{D}_{A/B} = \bar{D}_A/\bar{D}_B$ and $\alpha^{S}_{A/B} = \bar{S}_A/\bar{S}_B$ represent the diffusivity (or mobility) selectivity and the solubility selectivity, respectively.

1.3. Atomistic Models for Polyimides—State of the Art. Polyimides represent a class of stiff-chain polymers. In contrast to rubbery materials, there exist up to now only relatively few modeling results concerning membrane processes on stiff-chain polymers.[11,17−23] Some of the first packing models for PIs in particular have been developed by Hofmann and co-workers for a 6FDA polyimide and a specific poly(amide imide).[19] Both materials were synthesized and characterized a few years before by Fritsch and Peinemann.[24] Packing models consisting of about 2500−3000 atoms, representing polymer chains of 40−50 repeat units, were constructed. The main focus was at first the development of a strategy to pack amorphous chains containing aromatic moieties. A general equilibration cycle with up to 15 stages was developed. The suitability of the created packing models was tested by comparison of simulated and measured diffusivity and solubility values.

Configurations of melts of short oligomeric chains ($n = 4$) of two PIs have been investigated by Neyertz and Brown[25] with a new hybrid MC/MD technique. The same group[26] has also investigated structure and dynamics of a short oligomer chain for PMDA-ODA (i.e., Kapton (KAP), see below), a PI investigated here also and more recently, using longer chains of 40 repeat units, a series of copolyimides with the intension to characterize the influence of one of the polymer components on the free volume in the resulting packing models.[27] Also, glass transitions have been predicted for PI structures with MD simulation but with relatively short chains of only 10 repeat units.[28]

1.4. List of Selected PIs. The investigated polyimides are shown with their chemical structure formula for their repeat unit in Scheme 1 together with the acronyms we use in the following.

Table 1 contains typical names of the PIs that have been used in experimental investigations. The glass transition temperature (T_g) is a good experimental measure for the stiffness of the polymer backbone. In comparison with the experimental permeability values of oxygen in the PIs, also shown in Table 1, it can be seen that no simple correlation exists to the T_g values

and also that the experimental data are often afflicted with substantial deviation.

It was our intention to cover with the list of selected PIs both a large spectrum of permeability values, and to have also, with a comparatively small set of 10 polymers, the possibility for some potentially interesting comparisons between chemical structure of the repeat unit, atomistic packing structure, and gas transport data. Therefore, all but one of the PIs contain the same dianhydride moiety (6FDA). The exception KAP, with the dianhydride moiety PMDA, was included because this PI is a kind of reference material for which a relatively large amount of experimental data exist. The investigated polymers comprise materials with the highest-measured gas permeabilities, e.g., PI3 and PI4 (about 130 Barrer[42] for oxygen) for PIs, and also such a "slow" material as KAP with only about 0.5 Barrer. The high permeability and reasonable selectivity of PI3 (6FDA-durene) and PI4 were first described in 1987 in the patent of Hayes.[43] Recently, PI3 was chosen as dope material for asymmetric hollow fibers[44] with very good gas separation properties. T6 was prepared as part of a systematic study[45] of PIs, made by polycondensation of methyl-substituted diaminoterphenylenes with 6FDA. In this study, T6 showed the highest permeability of oxygen. The polyimide B4 represents to T6 the respective substituted biphenylene diamine moiety. The polymer B4 should show the same sterical effect of *o*-methyl groups in the diamine moiety relative to the imide group in the 6FDA dianhydride moiety. The polyimide BAAF has obtained already great attention as membrane material with excellent properties for gas separation. A good summary about recent work with BAAF may be found in refs 16 and 46. MDX was selected as part of a set of PIs (B4, MDX, T6) to study the influence of different spacer groups between 2,5-dimethyl-*p*-biphenylenes as part of the diamine moieties (i.e., without spacer, a methylene group, and 2,5-dimethyl-paraphenylene as spacer) on packing structure. Another set (BAAF, ODA, DDS) contains PIs with different spacers between unsubstituted biphenylenes in the diamine moiety. The comparison of ODA and KAP will allow us to study the influence of the dianhydride moiety (6FDA) and (PMDA). Also, ODA and KAP are still interesting materials for applications, e.g., KAP was used recently as advanced membrane material with polymeric nanoparticles.[47]

2. Modeling Details

2.1. Preparation of Packing Models. For each of the polymers in Scheme 1, at least three independent atomistic bulk models were realized utilizing the *Amorphous Cell* module of the *InsightII/Discover* Software of Accelrys, Inc.[48] The basic techniques used are described in ref 11. As a force field, the newly developed COMPASS force field of Accelrys[49,50] was used in all cases. The calculations have been performed on two SGI Octane two-processor workstations and an eight-processor SGI 2100. Details for the single-packing models are summarized in Table 2.

For the PIs, the initial *Amorphous Cell* packing procedure (i.e., a Theodorou−Suter algorithm)[51] using information on the conformation angle statistics and excluded volume effects was performed in each case with a single chain of 60−80 repeat units (about 4500 atoms). Larger systems in comparison to rubbery materials are necessary to see in stiff-chain polymers possible heterogeneities in the distribution of free-volume elements.

Table 2. Characterization of Single Packings

PI packings	no. monomer	no. atoms	MD at const	box length (Å)	density (g/cm^3)	FFV
PI3-1	76	4486	NpT	37.885	1.349	0.374
PI3-2	80	4722	NVT	38.484	1.334	0.371
PI3-3	80	4722	NVT	38.498	1.333	0.372
PI4-1	80	4482	NVT	37.987	1.353	0.372
PI4-2	80	4482	NpT	37.978	1.354	0.371
PI4-3	80	4482	NVT	37.967	1.356	0.370
T6-1	53	4507	NVT	36.936	1.315	0.328
T6-2	53	4507	NVT	36.863	1.323	0.324
T6-3	53	4507	NVT	36.912	1.317	0.327
B4-1	65	4487	NVT	37.585	1.318	0.356
B4-2	65	4487	NVT	37.880	1.288	0.370
B4-3	65	4487	NVT	37.883	1.289	0.369
BAAF-1	68	4490	NpT	38.479	1.472	0.375
BAAF-2	68	4490	NpT	38.492	1.470	0.375
BAAF-3	68	4490	NpT	38.333	1.489	0.368
MDX-1	63	4538	NpT	37.437	1.321	0.345
MDX-2	63	4538	NpT	37.468	1.318	0.347
MDX-3	63	4538	NpT	37.437	1.321	0.345
ODA-1	78	4526	NVT	38.057	1.430	0.346
ODA-2	78	4526	NpT	38.327	1.400	0.359
ODA-3	78	4526	NVT	37.932	1.444	0.339
PDA-1	80	3800	NpT	35.957	1.477	0.347
PDA-2	96	4514	NpT	38.305	1.465	0.358
PDA-3	96	4514	NpT	38.362	1.458	0.360
DDS-1	75	4502	NpT	38.231	1.464	0.347
DDS-2	75	4502	NpT	38.225	1.464	0.346
DDS-3	75	4502	NpT	38.259	1.460	0.348
KAP-1	115	4487	NVT	37.255	1.412	0.301
KAP-2	115	4487	NVT	37.174	1.421	0.297
KAP-1	115	4487	NVT	37.439	1.391	0.311

Because of this, in the present work, we consider the PI chains twice as long as those, which have been dealt with in some of the earlier works[11] on simulation of polyimides. Since all investigated PIs contain cyclic subunits (here phenylene rings) in the repeat units, the packing and equilibration stages have been much more laborious and time consuming than those in the case of other polymers. For PIs, the conventional packing algorithm may lead to artifacts of catenated phenylene rings or a spearing of side groups or backbone chains through ring substructures. Both effects are, of course, unacceptable and have to be avoided. To solve this technical problem, it is usually necessary to start with a very low initial packing density (typically 0.1 g/cm^3). For all PIs, this approach alone did, however, not lead to a complete avoiding of catenation and spearing events. Therefore, additionally a set of small molecules (e.g., 200−500 methanol molecules or 200−300 Si atoms) has been added randomly in the simulation box before the packing of the polymer was started to represent small obstacles preventing the respective growing polymer chains from ring catenations and spearings. The obstacle molecules are later, of course, to be removed again. Each removal procedure was followed by a structure relaxation using several hundred energy minimization iterations and several thousand MD steps with a force-field parameter-scaling scheme that was outlined in a recent publication.[52] The resulting packing systems were slightly below the respective experimental densities (about 10%). Therefore, at this stage the systems were compressed for 5 ps under high pressure at 1000−5000 bar via NpT-MD dynamics followed by a stimulated annealing procedure (NVT-MD simulations typically for 20 ps at 600 and 300 K). The stability of the packing was then checked with a subsequent 20-ps NpT simulation run at 1 bar. In some

Table 3. United Atom Representation of Penetrant Molecules in the Gusev−Suter TST

penetrant	σ_i (Å)	ϵ_i (kJ/mol)
O_2	3.46	0.980
N_2	3.70	0.790
CH_4	3.82	1.231
CO_2	4.00	1.881

cases the density decreased during this NpT run by more than 20% below the experimental values. In such cases, either the compression-stimulated annealing cycle was repeated or, if this procedure did not succeed, in further steps, NVT simulations had to be performed for the data production (see KAP and ODA in Table 6). Finally a longer MD run (NpT or NVT) of 300 ps was performed for each of the models in order to further improve the equilibration before using them for data production.

For ODA and KAP, only 95% of the experimental density was achieved at 1 bar. Slight problems such as this may happen for glassy stiff-chain materials (cf. refs 12, 48, and 53), particularly if the models are rather large as in the given case. These deviations may reflect minor errors of the parametrization of the respective polymers in the chosen force field, which influence the equilibration of the respective model. The whole procedure gets tougher the stiffer the chain and the larger the model is. In these cases of relatively low deviations of the model density at a 1 bar NpT-MD simulation from the respective experimental value, it is usually no problem to recompress the model to the experimental density and to run all subsequent MD simulations in the NVT mode.

2.2. Calculation of Gas Transport Data for Polyimides. We used the TST after Gusev and Suter[54−56] to study thermodynamics and transport of small gas molecules in the created polyimide packing models. With the help of an existing software tool,[57] we calculated diffusion coefficients (D) of small molecules in polymer matrixes, their solubility (S) in the matrix, and the respective permeability ($P = DS$). The calculation briefly consists of two steps. First, the free energy to insert a gas molecule in the polymer packing is calculated for all points on a fine grid laid over the packing cell. These data are then used to identify minimum-energy insertion sites ("holes") and to determine transition probabilities from site to site. The penetrant molecules were represented by Lennard-Jones spheres with force-field parameters given in Table 3.

Therefore, in this method, just the Lennard-Jones and not the Coulomb interaction energy is considered. Furthermore, it is assumed that the polymer packing does not undergo structural relaxation (e.g., resulting from torsional transitions) to accommodate an inserted particle. Therefore, as will be seen later, this simulation technique is restricted to small molecules (up to methane or even just N_2), which also do not show significant electrostatic interactions with the polymer matrix. From these interaction energy values, the solubility of the penetrant molecules is calculated (cf. refs 11, 55, and 56). In addition, the whole packing can be divided in regions of free volume (low interaction energy) and regions of densely packed polymer (high interaction energy). From this topology of the packing, energetically favorable transition paths between adjacent holes are identified. Each path between two local minima regions gets a Boltzmann factor of jump (transition) probability assigned, which results from proper averaging over the insertion energies determined in the area between the two holes. The jump probabilities are also influenced by the elastic thermal vibrations of the polymer matrix. This effect is considered in the Gusev−Suter TST via a Debye-like factor. The main material parameter utilized in this context is the Cartesian-smearing parameter $\langle\Delta^2\rangle$, the mean-squared displacement (MSD) (fluctuation) of a polymer atom from its average position. This parameter, with a value of a fraction of an angstrom, was obtained from a short MD run of 20 ps for the packed polyimides without penetrant molecules (see Table 4).

Table 4. Cartesian-Smearing Parameters

polyimide	Cartesian-smearing parameter $\langle\Delta^2\rangle$ (Å)
PI3	0.51
PI4	0.57
T6	0.61
B4	0.53
BAAF	0.48
MDX	0.55
ODA	0.44
PDA	0.44
DDS	0.48
KAP	0.46

The second, final step of the TST calculation represents a Monte Carlo simulation of gas diffusion by a "hopping" mechanism using the holes and the corresponding transition probabilities. To determine the diffusion coefficient of a gas in a polymer, we have calculated for every penetrant particle 1000 trajectories of a total diffusion time of 10^{-4} seconds that is necessary to fulfill the criterion of a random walk through the polymer matrix. The necessity of TST approaches to obtain diffusion coefficients for penetrants in PIs is nicely illustrated in Figure 1. The left panel shows that very long simulation times (greater than about 10 ns for oxygen and nitrogen and nearly 100−1000 ns for carbon dioxide) are necessary to reach the region of normal diffusion (characterized by the 45° slope in the log−log plots) and to fulfill the criterion of a random walk through the polymer matrix.

The right panel of Figure 1 shows MSD curves obtained from the longest MD simulation run of 6 ns in this study. There, in a well-equilibrated PI4 packing model, 10 oxygen, 10 nitrogen, and 10 carbon dioxide molecules had been inserted into different free-volume regions (for details see below). The system was equilibrated and then the NpT-MD simulation at $P = 1$ bar and $T = 300$ K was performed. In the time frame of about 100 ps up to 6000 ps, these directly simulated values are very well met by the MSD values calculated from the final step of the Gusev−Suter TST method (squares in Figure 1). Considering the computing time of roughly one month to calculate with a fully detailed atomistic MD simulation the temporary development of 1 ns of a PI packing model with about 5000 atoms on a single workstation CPU, Figure 1 also highlights the necessity to apply TST methods to determine diffusion coefficients of penetrant in these glassy polymer materials. Without TST methods, the necessary diffusion times would require much longer simulation times (factor 10^7) and are practically out of scope. Finally, in applying the TST, one should always keep in mind the simplifying assumptions of this approach. Where the MD simulation assumes only the validity of the force field and the applicability of classical dynamics on an atomistic level, the TST method involves an abstraction of the detailed

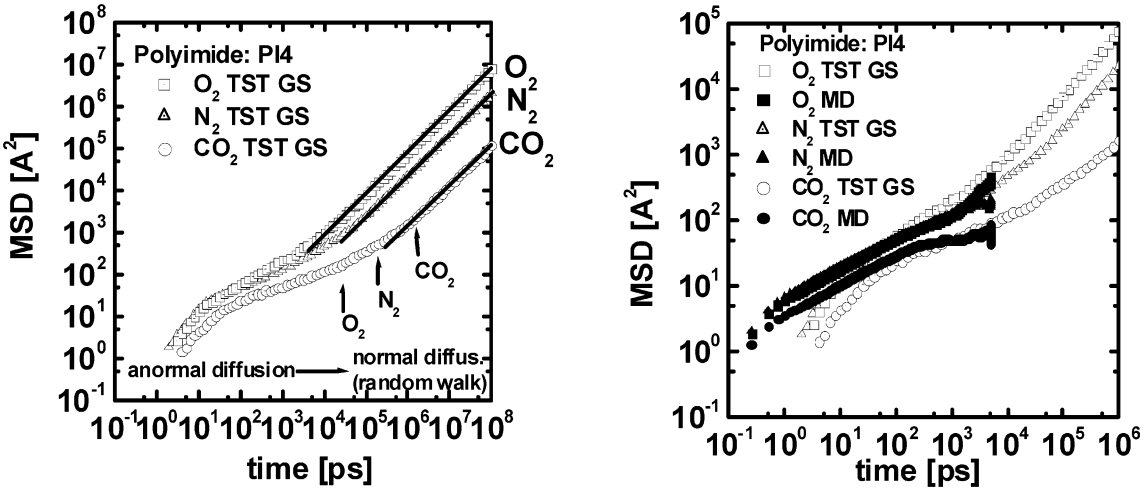

Figure 1. MSD of penetrant molecules in polyimide PI4 as function of simulation time. Left: MC simulation of gas diffusion by a "hopping" mechanism using sites and transition probabilities from Gusev−Suter TST. Right: Comparison of the MC result (open symbols) with direct atomistic NpT-MD simulation over a time of 6 ns (filled symbols).

Table 5. Calculated Properties for 20-mer Polyimide Chains Using RMMC Simulations

PI	ϵ^a	$\langle r^2\rangle^b$ (Å^2)	$C_n{}^c$	$\langle s^2\rangle^d$ (Å^2)	$\langle r^2\rangle/\langle s^2\rangle$	$\langle a_2\rangle^e$ (Å)
PI3	3.12	6102	10.0 ± 0.6	998	6.11	7.9 ± 0.1
PI4	3.15	5451	9.4 ± 0.5	877	6.22	7.7 ± 0.1
T6	2.96	12831	13.9 ± 0.9	2153	5.96	10.7 ± 0.2
B4	3.05	10773	14.1 ± 0.7	1677	6.42	10.7 ± 0.2
BAAF	3.01	7145	8.7 ± 0.4	1209	5.91	6.9 ± 0.1
MDX	3.03	7355	9.1 ± 0.4	1204	6.11	7.2 ± 0.1
ODA	3.20	7502	9.4 ± 0.3	1216	6.17	7.3 ± 0.1
PDA	3.27	7327	12.0 ± 0.4	1222	6.00	9.6 ± 0.2
DDS	3.55	6960	8.2 ± 0.3	1166	5.97	6.7 ± 0.1
KAP	3.60	13256	21.0 ± 0.5	2024	6.55	16.4 ± 0.3

[a] Relative dielectric constant of the medium. [b] Mean-squared end−end distance. [c] Characteristic ration. [d] Mean-squared radius of gyration. [e] Persistence length, representing the mean projection of the end−end vector on the directions of all backbone bonds.

short-time motions of the penetrant to a sequence of jump events in an (only) elastic responding polymer matrix. These preconditions of a TST approach always have to be proofed. This is done in turn by MD simulations, and this shows again the strong relationship between both methods.

3. Results and Discussion

3.1. Chain Properties. The "RIS Metropolis Monte Carlo" (RMMC) method, implemented in the InsightII/Discover software, was used to calculate some physical properties of single chains with 20 repeat units at room temperature. The RMMC method uses the force field to determine the conformational properties of the chain and does not require precalculated statistical weights for the polymer of interest, as the "classical" rotational isomeric state method. Results are shown in Table 5.

The ratio of mean-squared end−end distance $\langle r^2\rangle$ and the mean-squared radius of gyration $\langle s^2\rangle$ shows values around 6.0, typical for long Kuhn chains. The reported persistence length $\langle a_2\rangle$, representing the mean projection of the end−end vector on the directions of all backbone bonds, may be used as an indication for the stiffness of the polymers. There is no simple correlation with, e.g., the permeability of oxygen. From the studied 6FDA PIs, T6 and B4 have the largest persistence length. It is about 3 Å larger than for PI3 and PI4, the PIs with the highest P_{O_2} values. It should be noted that KAP, the studied PI with the lowest P_{O_2} value, has a still-higher persistence length than all the 6FDA PIs. Also from the comparison with ODA, it can be concluded that the PMDA moiety is stiffer than the 6FDA moiety. For the PIs with the largest persistence length, T6 and KAP, the calculations were repeated with a longer chain of 80 repeat units, and the same results have been found.

3.2. Density. The experimental density of the PIs was reproduced in the 300-ps NpT simulations for final equilibration with an accuracy of about 0.02 g/cm^3 for BAAF, MDX, PDA, DDS, and partly also for PI3, PI4, and ODA. For all other packing models, the density changed in respective simulations to slightly lower values; in that case, NVT simulations at fixed (experimental) density had to be executed.

3.3. Primary Transport Properties: Solubility, Diffusion, and Permeability. We used the TST after Gusev and Suter[54−56] to calculate for N_2, O_2, CH_4, and CO_2 the solubility (S) of the gas in the PI matrix and the diffusion coefficient (D) of the gases in the polymer matrixes (first results have been published in a conference proceeding).[58] At the beginning of a comparison of modeling results vs experimental data, we would like to discuss the obtained accuracy and the "quality" of reference data in the literature for one specific polyimide, PI4, as "typical" example.

Figure 2 presents predicted solubility values and literature data.[19,59,60] These data are shown as a function of the critical temperature T_c of the penetrants used, which is also a measure for the ease of condensation. Because molecules become more condensable with increasing diameter, simulation and experiment show that the solubility coefficient of the penetrants in PI4 gets larger as the molecular dimension increases. For oxygen and nitrogen, the agreement between simulation and experiment is very good, methane is still acceptable, and for CO_2, the calculated value is clearly too high. As can be seen from Table 6 also for the other PIs below, the simulated solubilities for CO_2 are always too high and the calculated diffusion coefficients (see below) are in general 1 or 2 orders of magnitude too small. This happens because in reality, the interaction of CO_2 with the glassy PIs is strong and can induce structural relaxations. This behavior "violates" the assumption of the TST after Gusev and Suter where the dynamics of the dissolved molecules is coupled only to the elastic thermal motion of the dense polymer and is treated

Table 6. Calculated and Experimental Solubility (*S*) and Diffusion Coefficient (*D*) for Oxygen, Nitrogen, Methane, and Carbon Dioxide

	S_{O_2} ((bar)$^{-1}$)		S_{N_2} ((bar)$^{-1}$)		S_{CH_4} ((bar)$^{-1}$)		S_{CO_2} ((bar)$^{-1}$)	
PI[a]	calcd	exp	calcd	exp	calcd	exp	calcd	exp
PI3[19,59,29]	3.6 ± 0.3	1.5 ± 0.5	2.5 ± 0.2	1.2 ± 0.2	11 ± 1	4.0 ± 1.8	92 ± 11	16 ± 13
PI4[19,59,60]	2.8 ± 0.1	2.4 ± 1.3	1.9 ± 0.0	1.5 ± 0.6	8.6 ± 0.3	4.6 ± 2.4	68 ± 5	13 ± 7
T6[45]	1.4 ± 0.1	1.8	0.8 ± 0.1	1.5	3.8 ± 0.5	5.9	36 ± 12	12
B4	2.9 ± 0.3		2.0 ± 0.3		9.2 ± 1.2		76 ± 10	
BAAF[8,16,33,34]	3.4 ± 0.3	0.9 ± 0.2	2.3 ± 0.2	0.7 ± 0.1	11 ± 1	1.6 ± 0.6	106 ± 18	4.4 ± 0.5
MDX[6]	2.0 ± 0.1	0.6	1.2 ± 0.0	0.5	5.8 ± 0.2	1.9	44 ± 1	6.8
ODA[6,8,60,33]	3.7 ± 0.1	0.9 ± 0.3	2.4 ± 0.1	0.5 ± 0.0	14 ± 0	1.3 ± 0.2	151 ± 8	5.9 ± 1.7
PDA[59]	3.9 ± 0.5	0.9	2.7 ± 0.4	0.7	15 ± 3	1.7	170 ± 42	5.0
DDS[39,40]	3.1 ± 0.4	0.5 ± 0.1	1.9 ± 0.2	0.4 ± 0.0	11 ± 2	1.3 ± 0.2	124 ± 41	5.1 ± 0.5
KAP[6,7,8]	3.3 ± 0.3	0.5 ± 0.1	2.0 ± 0.3	0.3 ± 0.0	15 ± 1	1.0 ± 0.1	211 ± 14	3.8 ± 0.6

	D_{O_2} (10^{-8} cm^2/s)		D_{N_2} (10^{-8} cm^2/s)		D_{CH_4} (10^{-8} cm^2/s)		D_{CO_2} (10^{-8} cm^2/s)	
PI[a]	calcd	exp	calcd	exp	calcd	exp	calcd	exp
PI3[19,59,29]	106 ± 79	67 ± 7	49 ± 45	24 ± 11	11 ± 1	4.0 ± 1.8	6.5 ± 8.8	31 ± 11
PI4[19,59,60]	106 ± 26	47 ± 22	41 ± 8	20 ± 8	8.6 ± 0.3	4.6 ± 2.4	2.8 ± 0.5	34 ± 17
T6[45]	73 ± 3	28	28 ± 4	8.3	9.2 ± 1.7	2.0	1.1 ± 0.9	9.1
B4[31]	58 ± 22		19 ± 9	2.7	6.6 ± 3.7		0.5 ± 0.3	
BAAF[8,14,16,33,34]	32 ± 4	10 ± 2	10 ± 2	3 ± 2	11 ± 1	1.6 ± 0.6	0.2 ± 0.1	8 ± 3
MDX[6]	46 ± 11	13	16 ± 4	27 ± 12	5.8 ± 0.2	1.9	0.8 ± 0.4	4.7
ODA[6,8,60,33]	7.5 ± 2.5	3.4 ± 0.8	2.0 ± 0.8	1.0 ± 0.2	0.5 ± 0.2	0.2 ± 0.05	0.03 ± 0.02	2.2 ± 1.5
PDA[59]	12 ± 9	3.5	2.7 ± 2.7	0.8	15 ± 3	1.7	0.04 ± 0.03	2.6
DDS[39,40]	18 ± 6	4.6 ± 1.3	5.2 ± 1.5	1.0 ± 0.1	1.7 ± 0.8	1.3 ± 0.2	0.09 ± 0.08	2.0 ± 0.1
KAP[6,7,8]	1.7 ± 0.9	0.7 ± 0.5	0.4 ± 0.3	0.2 ± 0.2	.09 ± .07	.05 ± .03	<0.005	0.5 ± 0.3

[a] References for the experimental values are given in the first column for every PI.

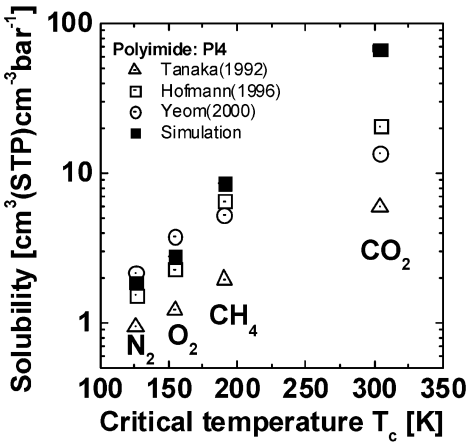

Figure 2. Comparison of simulated solubility values of N_2, O_2, CH_4, and CO_2 in polyimide PI4 with experimental data from literature

without regarding the occurring structural relaxations. The results for CO_2 show clearly the necessity to develop improved TST methods, which permit the matrix to be locally flexible to accommodate larger and stronger interacting penetrant molecules.[61] Only then will it be possible to calculate reasonable transport properties for CO_2 and larger permeate molecules.

For the upcoming comparison with experimental data, one has to pay, as described before, some attention to the actual measuring conditions. For the considered PIs, one finds in the literature actually no direct measurements for solubility coefficients $S(c) = S_0$ at such infinitely small penetrant concentration (see also eq 12) that would correspond directly to the situation in the TST calculation where one penetrant molecule alone occupies the whole packing model. Best experimental values for comparison are always solubility coefficients $S(c,p)$ determined directly from isothermal sorption measurements according to eq 1 of the equilibrium concentration at the smallest possible pressure. For PI4, only Tanaka et al.[59] have published such directly determined solubility coefficients, which differ (for the convenience of the measurement with certain gases) in the pressure value (for O_2 and N_2 at $p = 2$ atm and for CH_4 and CO_2 at $p = 10$ atm). The other experimental solubility coefficients for PI4 in Figure 2 represent actually "only" effective values S_{eff}, see eq 10, calculated from the effective permeability coefficient P_{eff} and respective diffusion coefficient D_{eff}, defined in eqs 8 and 9, and measured in the time-lag experiment. Also in these experiments the pressure conditions are in general not standardized, so the permeation experiments, reported in Hofmann et al.,[19] were performed at $p = 1$ atm, while the data of Yeom et al.[60] were measured at a higher feed pressure of 10 atm. This exemplary discussion of specific conditions and methods under which the experimental data were obtained may explain to a large part the typical scatter of experimental data, found in the literature, and also highlights the necessity to develop more standardized conditions for these measurements.

Figure 3 presents, for example, PI4, the comparison between simulated and experimental diffusion coefficients. Our simulated values, on the basis of the TST model, correspond in principle to constant diffusion coefficients D_0 at infinite dilution, see eq 11, which should be observed in permeation experiments at very low upstream pressures. The experimental value of Tanaka et al.[59] represents in fact a calculated averaged diffusion coefficient $D_{mean} = \bar{P}/S(c,p) \approx \bar{D}$, determined from the averaged permeability coefficient $\bar{P}$, a steady-state quantity, and the equilibrium solubility coefficient $S(c,p)$, which is a good approximation for the averaged solubility coefficient $\bar{S}$ in a membrane, defined in eq 7. The other two experimental data sets in Figure 3 represent actual time-lag values D_{eff} after eq 9, measured at different pressures. The diffusion coefficients from TST calculations for nitrogen, oxygen, and methane agree within a factor of 3−5 to the respective experimental average values. The particularity of the CO_2−polyimide system is indicated experimentally by

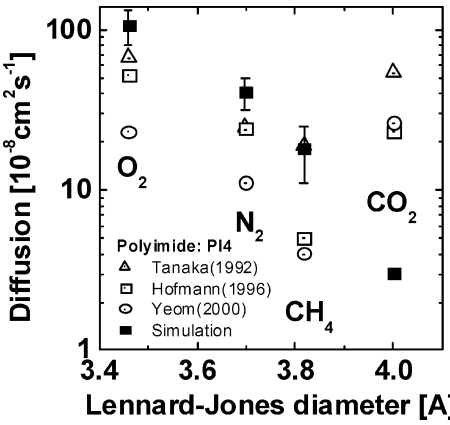

Figure 3. Comparison of simulated diffusion coefficients of N_2, O_2, CH_4, and CO_2 in polyimide PI4 with experimental data from literature.

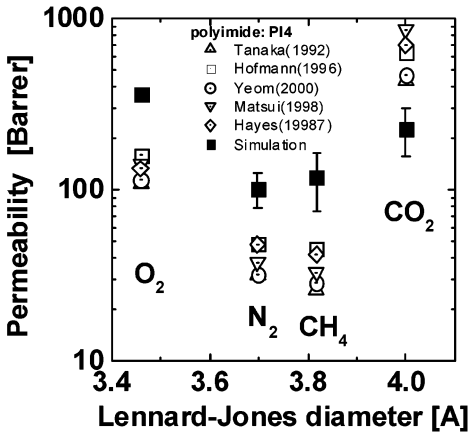

Figure 4. Comparison of simulated permeability values of N_2, O_2, CH_4, and CO_2 in polyimide PI4 with experimental data from literature.

the larger diffusion coefficient compared to the smaller value for methane. This behavior, probably related to anisotropic geometry of the molecule combined with stronger interactions that may also induce plasticization effects, is not accommodated in the applied TST model, which predicts for CO_2 a much smaller diffusion coefficient than for methane.

As a final step in the discussion of transport properties for PI4, Figure 4 shows the predicted permeability values in comparison to experiments. Experimental data for permeabilities are more often reported than *D* and *S* values. It is typical that one finds for permeability values more "independent" experimental data sets. The data are normally measured with the time-lag technique, see eq 8. This is also the case for PI4, where two further references with permeability measurements can be found in the literature.[62,43] It should be mentioned that Yeom et al.[60] used a special method that allowed them to measure simultaneously the flux transient and the permeate composition. For O_2, N_2, and CH_4, experimental and calculated permeation values agree in the same order of magnitude. This is even true for CO_2 as a consequence of a systematic error compensation in the product out of *S* and *D*. Also for the other PIs it was found that for CO_2 the calculated diffusion coefficients (see Table 6) are about an order of magnitude too small, where the calculated solubilities are dramatically higher than the experimental values.

Our results concerning the comparison of simulated and experimental diffusivity and solubility data for the

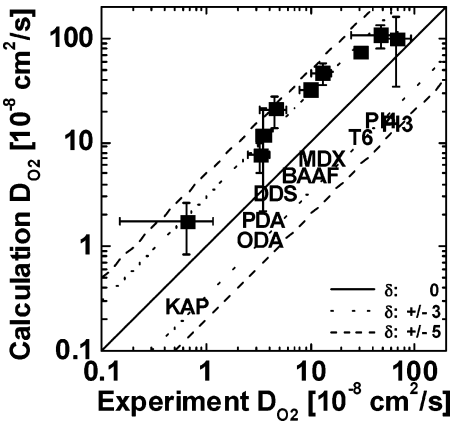

Figure 5. Comparison of simulated diffusion coefficients of O_2 in polyimides with experimental data.

specific example PI4 can be generalized in principle to the whole set of investigated PIs.

Table 6 shows that the deviation for O_2 and N_2 is in general in the range of a factor of 1−4, with a few exceptions (factor of 5−7) for KAP and DDS, and to a lesser extent (up to 5), for ODA. This range of deviation is in accordance with recent simulations results for rubberlike materials and earlier simulations for polyimide membranes.[11] The larger deviation for ODA and KAP is probably related to an insufficient parametrization of the ether oxygen in the diamine moieties by the COMPASS force field under *InsightII*.[63]

As an example for the quality of predictions within the set of PIs, Figure 5 shows the oxygen diffusivities for the nine PIs (excluding B4) for which experimental data exist (for references see Tables 6 and 7). Error bars are given to show the scatter of the calculated values (from the set of three independent packing models) and also of the experimental data in cases where more than one independent measurement or preparation of the membrane could be found in the literature. By comparison of these experimental error bars, one should have in mind that the number of "independent observations" per PI differs (PI3, 4; PI4, 3; T6, 1; BAAF, 4−5; MDX, 1; ODA, 4; PDA, 1; DDS, 2; and KAP, 2−3). So, points with smaller error bars may seem to be measured more accurately, but in fact, simply less data were available. The additional problem that becomes manifest when searching in the literature for experimental solubility and diffusion data of the investigated PIs was already discussed for the specific example PI4. Despite the fact that in most cases the measurement is performed at a temperature of 35 °C, the pressure of the solubility measurement varies often from reference to reference. In general, the measurements are not performed under such a low pressure, corresponding to the practical "zero concentration limit" in the calculation of the Gusev−Suter TST. Further, most diffusion coefficients in the literature are determined in time-lag experiments as effective values D_{eff}, and the solubilities are often calculated from the permeability using eq 10. The average over these "diverse" sources of experimental information are also expressed in the experimental values in Figure 5 or Table 6 and explain the varying extension of the respective error bars.

We observe that the diffusion coefficient for O_2 changes by about 2 orders of magnitude in the set of PIs, from KAP with a diffusion coefficient of about 0.6 $\times$ 10^{-8} cm^2 s^{-1} up to 67 $\times$ 10^{-8} cm^2 s^{-1} for PI3. Over

Table 7. Calculated and Experimental Values for the Ideal Gas Selectivity $\alpha^{id}_{O_2/N_2} = P_{O_2}/P_{N_2}$ (see eq 13) for O_2/N_2 separation on the Investigated Polyimides and Their Diffusive ($\alpha^{D}_{O_2/N_2} = \bar{D}_{O_2}/\bar{D}_{N_2}$) and Solubility ($\alpha^{S}_{O_2/N_2} = \bar{S}_{O_2}/\bar{S}_{N_2}$) Dependent Factors

	$\alpha^{S}_{O_2/N_2}$		$\alpha^{D}_{O_2/N_2}$		$\alpha^{id}_{O_2/N_2}$	
PI[a]	calcd	exp	calcd	exp	calcd	exp
PI3[19,43,44,59,29]	1.4 ± 0.1	1.3 ± 0.5	2.7 ± 0.8	3.1 ± 0.9	3.9 ± 1.1	3.5 ± 0.3
PI4[19,43,59,60,62]	1.5 ± 0.0	1.5 ± 0.2	2.6 ± 0.2	2.3 ± 0.3	3.6 ± 0.4	3.3 ± 0.3
T6[45]	1.7 ± 0.1	1.2	2.7 ± 0.5	3.4	4.6 ± 0.7	4.1
B4[32]	1.5 ± 0.1		3.2 ± 0.5		4.7 ± 0.8	3.7
BAAF[8,16,33,34]	1.5 ± 0.0	1.4 ± 0.4	3.2 ± 0.3	3.4 ± 0.5	4.8 ± 0.4	4.6 ± 0.1
MDX[6,32]	1.6 ± 0.0	1.1	2.9 ± 0.1	4.3	4.7 ± 0.2	4.5 ± 0.5
ODA[6,8,60,33,36,37,38]	1.5 ± 0.1	1.7 ± 0.5	4.0 ± 0.8	3.5 ± 1.4	6.1 ± 1.2	5.5 ± 1.1
PDA[59,36,37]	1.4 ± 0.1	1.2	4.9 ± 1.0	4.3	6.8 ± 1.4	5.4 ± 0.1
DDS[39,40,41]	1.6 ± 0.0	1.3 ± 0.2	3.5 ± 0.1	4.3 ± 0.8	5.6 ± 0.3	5.8 ± 0.5
KAP[6,7,8,37,38]	1.7 ± 0.0	1.6 ± 0.3	4.8 ± 0.8	4.0 ± 1.2	8.0 ± 1.3	6.2 ± 1.5

[a] References for the experimental values are given in the first column for every PI.

this large range, the calculated D_{O_2} values agree to a factor of 3−5 with experimental data. Further, it can be seen that the calculated diffusion values are mostly higher than the experimental ones. We assume that this trend is due to the difficulties in experimentally obtaining really pure and ideal amorphous polymeric materials (in addition to the already discussed problems of accurate measurements of D and S values). There are several issues. For polyimides, as for many other stiff-chain glassy polymers, the problem of a residual solvent being strongly absorbed in a potentially considerable part of the free volume is of particular importance. These solvent traces may to a certain extent be removed by immersion in methanol of as-cast films. Recently, Nagai et al.[64] have studied in detail the effect of methanol conditioning on the transport properties of a glassy polymer and concluded that regardless of film preparation history and age, the methanol immersion increases the nonequilibrium excess free volume in the glassy polymer membrane, with the consequences of higher permeability for, e.g., oxygen, propane, and *n*-butane, higher solubility coefficients for the higher hydrocarbons, and higher diffusion coefficients at low *n*-butane concentration. A strong permeability enhancement by penetrant-induced conditioning, due to considerable increase in diffusion, was also observed[65] for the polyimide BAAF at CO_2 pressures greater than 10 atm where, a further problem, the conditioning is interrelated with strong plasticization effects. Further, it was confirmed that residual solvent could still be detected by TGA in actual PI membranes, which were prepared following standard literature procedures for synthesis and film preparation.[66] This is due to the extremely high boiling point of the solvents necessary in the synthesis, like NMP, which can practically not be removed completely. This fact is in line with higher permeability values for PI3 and PI4 films,[19] reported after rather long methanol conditioning in the final preparation, to remove the high-boiling solvent, in contrast to membranes cast after the "normal" procedures in the literature, e.g., in ref 59. Also, for the assessment of experimental solubility values, the residual solvent issue is certainly of importance.

After this "critical" discussion of experimental conditions and sample quality, it should finally also be mentioned that the relations between the gas molecule insertion energies determined directly from the packing models and the quantities D_{calc} and S_{calc} are highly complex. Therefore, even relatively small errors of the insertion energies, which are determined by the quality of a respective model, may lead to rather high errors for D_{calc} and S_{calc}. Because of both reasons, the experimental uncertainties and the simplicity of the model assumptions, it is at present generally accepted to consider a coincidence between measured and simulated diffusivity and solubility values within a factor of 3−5 as reasonable.

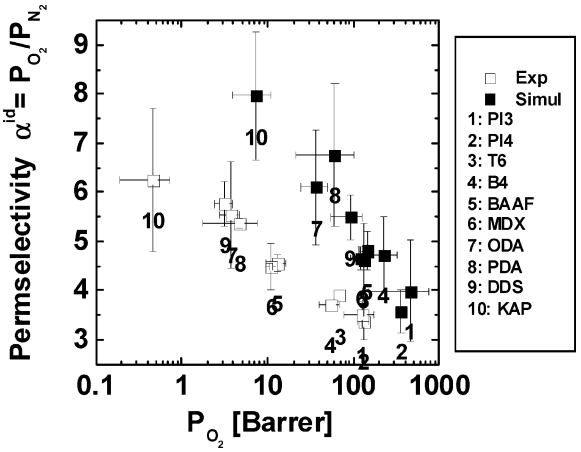

Figure 6. Permselectivity for O_2/N_2 separation vs oxygen permeability for PIs, simulation (filled symbols) and experiment (open symbols).

3.4. Selectivity. A significant improvement to former results could be achieved for the calculated O_2/N_2 selectivity values and trends, presented in Table 7.

This is probably a consequence of further improved equilibration strategies and of the application of the new force field COMPASS. This force field is known to be better adjusted to density-related properties in polymers. In older investigations on polyimides, selectivity values showed considerably larger deviation from experiment.[11] In former simulation studies it was not possible to find, especially for glassy polymers, such comparatively consistent trends for the change of selectivity as now for the polyimides shown in Table 7.

In good accordance with the experiment, we see in Figure 6 for the modeled data that with decreasing permeability P for oxygen, the permselectivity for oxygen over nitrogen $\alpha_{O_2/N_2} = P_{O_2}/P_{N_2}$ is increasing and, further from Figure 7, that this increase is a result of the different diffusivities of both compounds in the specific PIs.

The diffusion selectivity $\alpha^{D}_{O_2/N_2} = \bar{D}_{O_2}/\bar{D}_{N_2}$ (Figure 7, left) shows the same variation as the permselectivity P_{O_2}/P_{N_2}, while the solubility selectivity $\alpha^{S}_{O_2/N_2} = \bar{S}_{O_2}/\bar{S}_{N_2}$ (Figure 7, right) varies much less for the set of polyimides. We see that for the set of PIs, the diffusion

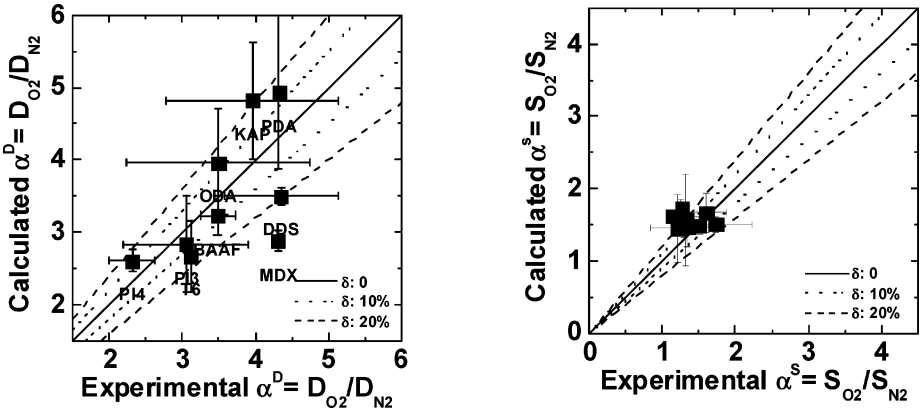

Figure 7. Comparison of simulated results with experimental data for the two factors determining the O_2/N_2 permselectivity in PIs. Left: Diffusion selectivity $\alpha^D_{O_2/N_2}$. Right: Solubility selectivity $\alpha^S_{O_2/N_2}$. It can be seen that diffusion selectivity can be calculated on average within 20% deviation from experiment.

selectivity can be calculated on average within 20% deviation from experiment. This would be already an acceptable level for the computer-aided molecular design of new membrane materials, which is expected to become reality soon. Further, we see in the left plot of Figure 7 the range of diffusion selectivities from such high values as 4.8−4.9 for KAP and PDA to the smallest values of 2.6−2.7 for PI4, PI3, and T6. In contrast, the representation of the other factor of the permselectivity, the solubility selectivity $\alpha^S_{O_2/N_2}$, in the same scale of coordinates shows a spotlike accumulation of points around a value of about 1.5. The deviation from experiment of the calculated solubility selectivities is similar as for $\alpha^D_{O_2/N_2}$.

Further, a trend of decreasing diffusivity selectivity with increasing O_2 diffusion coefficient is seen for the studied polyimides, both from experiment and simulation, in the order KAP ≈ PDA > ODA > DDS > BAAF ≈ MDX > T6 ≈ PI4 ≈ PI3. Looking at the chemical structure of the polymers, it can be recognized that PI3 and PI4, the materials with the largest O_2 diffusion and smallest diffusion selectivity $\alpha^D_{O_2/N_2}$, have a more rigid or bulky segment in the diamine part than KAP, PDA, or ODA. In the general understanding of the correlation of membrane structure and membrane properties, a rule of thumb says that more rigid and bulky segments in the polymeric backbone will likely inhibit more intersegmental packing of polymeric chains because of hindered backbone mobility. Thus, the inhibition of backbone mobility may result in an increasing free-volume fraction and therefore in a more open matrix with larger intersegmental openings for the diffusion of gas permeates. Further, it is assumed that if the membrane structure is opened extensively enough, the separation capability for such similar permeate molecules as oxygen and nitrogen is reduced because less "specific" interactions are possible with the matrix structure. The result is a decreasing selectivity. How far this common explanation is accurate for PI materials can be investigated with a more detailed analysis of the free volume.

3.5. Free-Volume Analysis. The size and the distribution of-free volume regions in amorphous polymers are of great importance for the transport behavior of small- and medium-sized penetrant molecules in these materials. Experimentally, the free volume of a polymer may be characterized with positron annihilation lifetime spectroscopy (PALS)[67−69] as the most common method

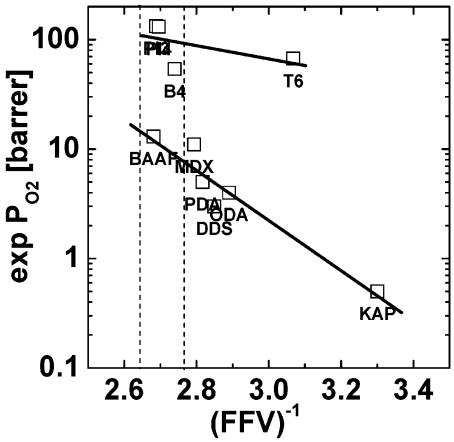

Figure 8. Experimental permeability of oxygen as function of the FFV derived from packing models. The region between dashed lines contains PIs with similar FFV, but oxygen permeability values differ by about 1 order of magnitude (see, e.g., BAAF to PI3/PI4 respectively).

where the correlation between measured lifetime of *o*-positronium and size of the void volume is used, but also other probe methods (inverse gas chromatography, ^{129}Xe NMR) are applied. The simulated atomistic bulk models allow now an "alternative" accurate determination of geometrical quantities characterizing the structure of segmental packing. Table 2 gives as example also the fractional free volume (FFV), calculated purely geometrically from the present packing models. It is now possible to correlate such a structural parameter, derived from the packing models, with experimental gas transport data. Figure 8 shows the plot of the experimental permeability for oxygen vs the FFV. The idea to plot log(*P*) as function of the inverse FFV goes back to theoretical (QSPR-like) consideration of diffusion in rubbery polymers. Fujita[70] had derived an exponential relation of diffusion *D* and the inverse FFV

$$D = A_d R T \, e^{(-B_d/\mathrm{FFV})} \qquad (14)$$

where *R* is the gas constant, *T* is the temperature, and A_d and B_d are polymer- and penetrant-dependent parameters. Lee[71] used this result and developed a similar empirical correlation for the permeability *P* provided that the solubility *S* is not strongly FFV dependent. Recently, the correlation was confirmed also by Alentiev and Yampolski.[72]

Figure 8 shows on one hand, in accordance with eq 14, the general tendency that the oxygen permeability is increasing with increasing FFV, but we find also, at very similar FFV values, oxygen permeability values differing by about 1 order of magnitude (see, e.g., BAAF to PI3/PI4, respectively). Figure 8 suggests therefore that not only the *total* value of the FFV but also, as we will show below, the *configuration* of free-volume elements into smaller and larger regions may be important for the permeability of a specific PI. A similar conclusion was recently drawn by evaluation of gas transport through two stereoisomeric polynorborenes.[73]

A recently developed program[52] was used to estimate from validated packing models the *size distributions* of free-volume elements, which may be covered by a spherical penetrant of certain radius. This free volume is determined by first superimposing a fine grid over the cubic packing, and then, at every point of the grid, it is tested if an overlap occurs between a hard sphere test particle (representing the penetrating molecule) and any atom of the polymer (represented also by a corresponding hard sphere). The result is a classification of grid points as "occupied" or "free". Next, the connectivity of the "free" grid points is considered, and connected "free" grid points are collected into groups, which represent individual holes. This is done in two ways. In the first approach (named *V_connect*), the simple topological criterion is that every point of a group has at least one next neighbor who is also member of this group. This approach identifies holes, which may be of complex shape and of large size. In a second approach (named *R_max*), a precalculated information for every grid point, its shortest distance to a polymer atom, is used to group. Among these distances, local maxima are defined by calculating the related gradient. Then each grid point of the free-volume regions is assigned to its nearest local maximum. The *R_max* approach may dissolve larger free-volume regions of elongated or highly complex shape into smaller "local" regions. The second approach was introduced to come closer to the situation of PALS spectra where the positron probe particle can obviously not completely sample very large holes of complex topology.

In both approaches, the number of lattice cells belonging to a hole multiplied by their cell volume was used as a measure for the volume of this hole. Finally, a correction is necessary to get the value for the *total* occupied volume by the probe molecules and not only the occupied part with respect to the center of the probe. Depending on the number of "occupied" next-neighboring grid points, for every "free" grid point in the hole, an appropriate volume segment of the probe sphere was added to the volume. The correction was zero, when all next-neighbor sites of a the considered grid point were also "free" (nonsurface region of a hole), and it would be the total volume of the probe sphere when the considered "free" site would be surrounded only by "occupied" grid points. The obtained volume of each hole was converted to an equivalent sphere, the radius of which is taken as a measure for the average linear dimensions of the respective hole.

Calculated size distributions (*V_connect* approach) of the free-volume regions accessible for a test particle of oxygen size are given for all investigated PIs in Figure 9. For each polymer, the distribution was determined from three packing models used in the calculation of the transport properties. The data set is still small, and

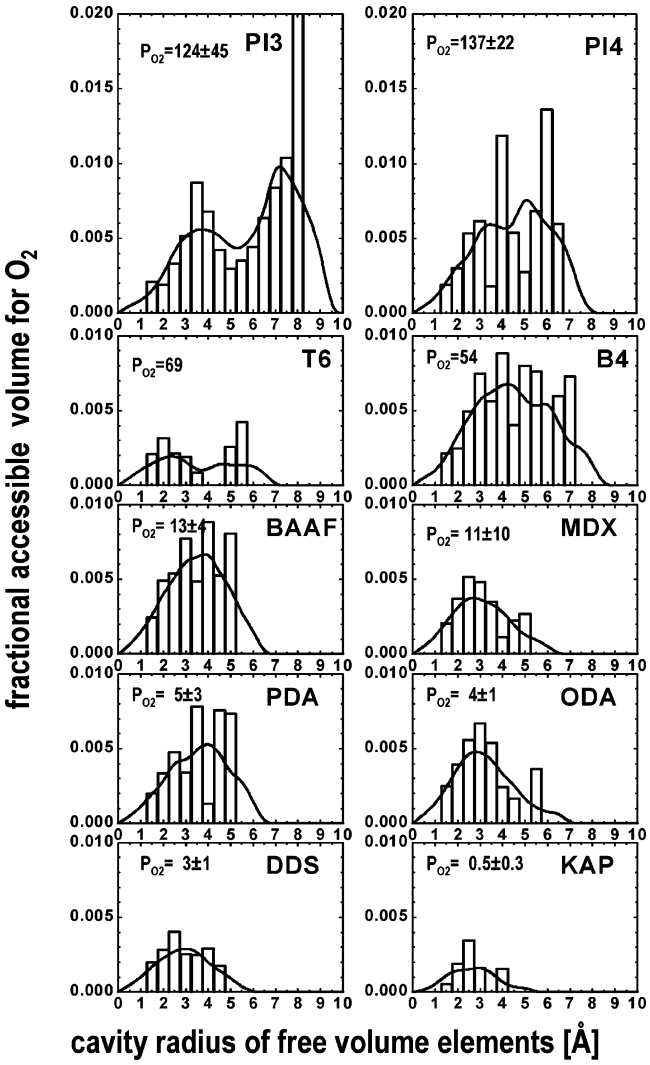

Figure 9. Bar-graph size distribution of free-volume elements accessible for O_2 calculated with the *V_connect* approach from three packing models per PI. The lines present a 5-point smoothing curve.

therefore the distributions are not smooth. They show relatively strong fluctuations. Therefore, a simple five-point smoothing was applied and is presented as a line.

The smoothed distributions of BAAF, B4, PI3, and PI4, i.e., the PIs with the largest FFV of the investigated set (see the dashed region in Figure 8), are compared in Figure 10.

All four PIs show a maximum distribution for cavities with a radius of about 3−4 Å. The distributions for the "fastest" 6FDA polymers PI3, PI4, and B4 (experimental O_2 permeability 50−130 Barrer) show additionally a distinct shoulder at cavity radii larger than about 6.0 Å. The polyimide BAAF on the other hand has a similar large free volume (see Figure 8) as the "fast" 6FDA PIs but belongs from the shape of the distribution to the set of very similar curves for MDX, ODA, DDS, and PDA with more or less a single peak (see Figure 9). This "group" of 6FDA PIs has oxygen permeabilities of only 3−13 Barrer.

The interpretation of the observed free-volume distributions in relation to the chemical structures for the investigated PIs suggests at present the following picture: The highest oxygen permeabilities are found for the PIs with an additional "shoulder" or peak in Figures 9 and 10, representing the presence of larger

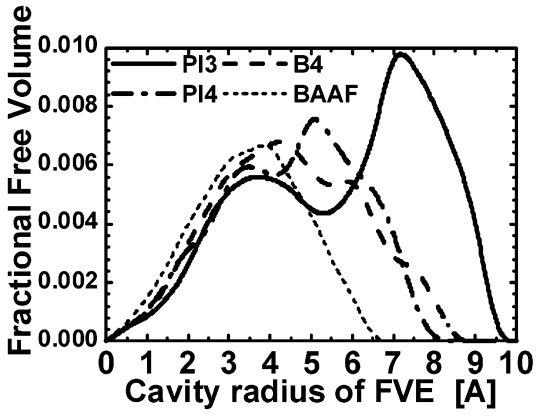

Figure 10. Comparison of the smoothed (see Figure 9) size distributions of free-volume elements accessible by O_2 for four PIs.

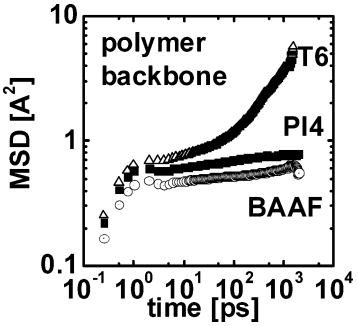

Figure 11. Averaged MSD of backbone atoms in the polyimides T6, PI4, and BAAF from NpT-MD simulation (T = 300 K, P = 1 bar) of a time of 2 ns.

cavities with radii > 5−6 Å. For their creation, two factors in the structure of the diamine moiety (see Scheme 1) seem to be important: (i) the methyl substitution in the ortho position to the amine groups (see PI3, PI4, B4, also T6 and MDX) which clearly inhibits the backbone mobility at the C−N bond between anhydride and diamine moieties but (ii) simultaneously also the "stiffness" of the amine moiety in itself, e.g., by conjugation of the aromatic rings. The second presupposition is, e.g., not fulfilled in MDX, where a flexible −CH2− group bridges the two phenyl units. Therefore, despite the fact that in MDX *o*-methyl groups exist, the FFV distribution lacks the shoulder at higher radii and the permeability for oxygen is only about 10 Barrer, similar to values for PIs without the ortho-substituted methyl groups as in BAAF, ODA, DDS, and PDA.

The also "*o*-methyl-substituted" polymer T6, with the long terphenylene diamine moiety, seems to be a special case. Despite the fact that the oxygen permeability is higher than in the sterically similar B4, the FFV values in Table 1 are smaller for T6 and also the distribution function in Figure 9 has a lower area and does not contain the "characteristic" larger free-volume regions at a radii > 6 Å. As explanation for this specific behavior we assume at present a specifically high chain mobility. Figure 11 shows the averaged mean square displacement (MSD) curves for atoms in the backbone of the *o*-methyl-substituted polymers T6 and PI4 and, as reference, also for BAAF, a polymer without this substitution pattern. The backbone atoms in T6 have moved in a period of 1 ns on average two times further than in the other two PIs.

Finally, the accuracy of the calculated distribution functions could recently be validated a bit better. For

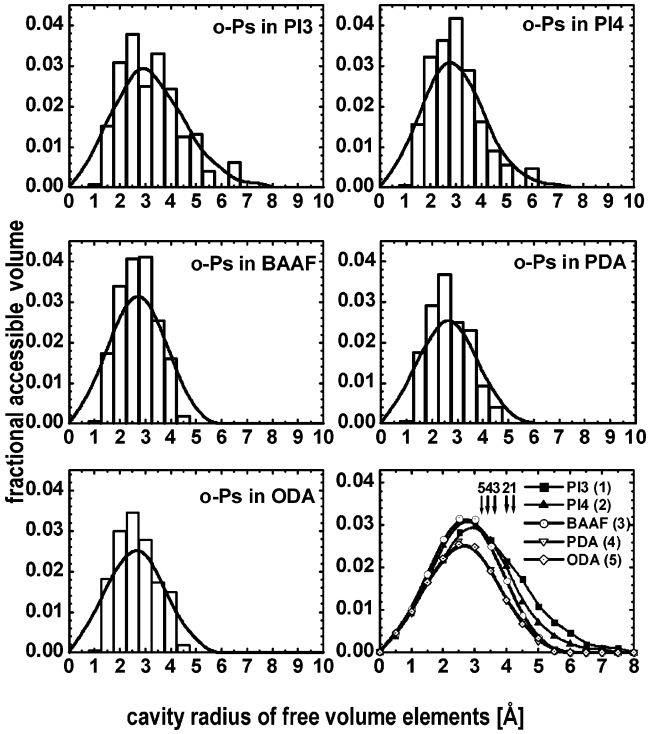

Figure 12. Size distributions of fractional free volume elements accessible for *o*-positronium probe (*R_max* approach) presented as a bar graph and 5-point smoothing curve. The bottom right graph shows a comparison of the smoothed curves for five PIs and additionally, marked with arrows, the maximum of a Gaussian size distribution, which can be derived from PALS data.[72]

five of the PIs listed in Scheme 1, there exist experimental PALS data.[74] For these PIs, the free-volume distribution functions accessible for a hydrogen atom (radius = 1.1 Å), which may represent in size the positronium particle of the experiment, have been calculated from the packing models and are shown in Figure 12.

In contrast to the results in Figures 9 and 10, in these calculations, the *R_max* approach has been applied. The maximum of the distribution is at about 2.5−3.5 Å. Next to this main peak a slight shoulder is found additionally for PI3 and PI4 at 6.0−6.5 Å The arrows in Figure 12 mark the maximum of a Gaussian size distribution, which can be estimated from the experimental lifetime and intensity of *o*-positronium decay in the polymer materials. Despite an absolute deviation of about 1 Å, the simulation result is in agreement with experiment concerning the trend, ODA has the smallest value and the "fast" polyimides PI3 and PI4 show the largest values.

4. Conclusion

With molecular modeling it was possible to determine gas solubilities and diffusivities for oxygen and nitrogen in the set of studied polyimides in good agreement with experiment (factor 1−4). The applied TST method (Gusev−Suter) does not work well, as expected, for CO_2 and other larger molecules because the stronger interactions of these penetrants with the PIs induces structural relaxations in the polymer matrix which are not considered in the TST.

The selectivity trends for O_2/N_2 are well described in accordance with experimental findings. In contrast to former modeling studies where selectivity values scat-

tered considerably, our simulation result shows for the set of PIs the same general trend as observed in experiments, i.e., for decreasing permeability of oxygen an increasing permselectivity for oxygen over nitrogen $\alpha_{O_2/N_2} = P_{O_2}/P_{N_2}$, which is mainly determined by the ratio of the diffusion coefficients D_{O_2}/D_{N_2} in a specific polyimide because the solubility ratio S_{O_2}/S_{N_2} is, at least for the investigated set of PIs, very similar.

The simulated packing models allow a very detailed determination of structural parameters either as a single parameter, like the accessible volume for certain penetrant molecules, or as a distribution function of free-volume elements. Characteristic of the "fast" 6FDA PIs in the investigated set seems to be on the structural level a wider distribution of free-volume regions with an additional peak or shoulder at larger radii as compared to the "normal" PIs. The constitutive structural element seems to be the methyl groups in ortho position to the imide group on the aromatic diamine moieties.

Finally, it should be said that our approach so far was mainly focused on the "static" aspects of free volume. But also "dynamic" properties of the free volume play a certain role. In particular dynamic relaxations, especially the secondary (or sub-T_g) relaxations, which are more localized than the glass transition, may have some influence for our PI materials. In principle, it is possible to observe with long MD simulations how segmental relaxations of flexible side groups in the polymer packing influence the lifetimes of the temporary channels through which the diffusive jumps of individual penetrant molecules take place. Some initial investigations have been undertaken also by our group for two other PIs.[12] It was found, e.g., that a stiff side group (naphthalene) controlled channels with often a much longer lifetime (up to more than a few ns) than the average residence time of a penetrant molecule in a local hole (up to a few hundred ps), resulting in back and forth jumps. Other channels were influenced by flexible side groups (like methyl groups), which lead to shorter lifetimes, and a local diffusive behavior comparable with the case of rubbery polymers. In principle, it should be possible to detect the frequencies of, e.g., rotations of methyl groups, phenyl rings, etc., which control the opening and closing of the temporary channels. These frequencies are certainly specific to the structure of the repeat unit of the PI. For the considered set of 10 PIs, a systematic study would have been beyond the scope of the present paper, but such investigations are planned for the future. A last argument for the strong structural dependence is the influence of isomerism, as, e.g., observed by Coleman and Koros[75] between the meta-connected isomer and BAAF (with the para-bounded diamine). A suppression of the segmental mobility for the meta isomer was indicated by an increase in the sub-T_g transition temperature (measured with dynamic mechanical thermal analysis). This higher steric resistance for the BAAF meta isomer increased slightly the density, reduced the fractional free volume, and lead to smaller solubility and diffusion coefficients for oxygen. This example shows that chain packing and chain motion seems to be interrelated and influence both the gas-transport properties of a certain polyimide. But nevertheless we are convinced that there is a rather strong correlation between the free-volume distribution of a glassy polymer and its transport properties, especially if the polymers belonging to the same class.

Acknowledgment. The authors thank Sandrine Fudaley (Air Liquide) for the preparation of some initial packing models, Yuri Yampolski (A.V. Topchiev Institute, Moscow) for assessing experimental PALS data, and Martin Böhning (BAM, Berlin) for valuable discussions. The research was supported by the European Commission "Growth" Program, "PERMOD—Molecular modeling for the competitive molecular design of polymer materials with controlled permeability properties", Contract #G5RD-CT-2000-200.

References and Notes

(1) *Polymeric Gas Separation Membranes*; Paul, D. R., Yampolskii, Yu. P., Eds.; CRC Press: Boca Raton, 1994.
(2) Robeson, L. M.; Burgoyne, W. F.; Langsam, M.; Savoca, A. C.; Tien, C. F. *Polymer* **1994**, *35*, 4970−4978.
(3) Langsam, M. In *Polyimides: fundamentals and applications*; Ghosh, M. K., Mittal, K. L., Eds.; Marcel Dekker: New York, 1996.
(4) Li, Y.; Wang, X.; Ding, M.; Xu, J. *J. Appl. Polym. Sci.* **1996**, *61*, 741−748.
(5) Mi, Y.; Stern, S. A.; Trohalaki, S. *J. Membr. Sci.* **1993**, *77*, 41−48.
(6) Hirayama, Y.; Yoshinaga, T.; Kusuki, Y.; Ninomiya, K.; Sakakibara, T.; Tamari, T. *J. Membr. Sci.* **1996**, *111*, 169−182.
(7) Kim, T. H.; Koros, W. J.; Husk, G. R.; O'Brien, K. C. *J. Membr. Sci.* **1988**, *37*, 45−62.
(8) Tanaka, K.; Kita, H.; Okano, M.; Okamoto, K. *Polymer* **1992**, *33*, 585−592.
(9) Müller-Plathe, F. *Acta Polym.* **1994**, *45*, 259−293.
(10) Gusev, A. A.; Müller-Plathe, F.; van Gunsteren, W. F.; Suter, U. W. *Adv. Polym. Sci.* **1994**, *16*, 207−247.
(11) Hofmann, D.; Fritz, L.; Ulbrich, J.; Schepers, C.; Böhning, M. *Macromol. Theory Simul.* **2000**, *9*, 293−327.
(12) Hofmann, D.; Fritz, L.; Ulbrich, J.; Paul, D. *Comput. Theor. Polym. Sci.* **2000**, *10*, 419−436.
(13) Stern, S. A.; Krishnakumar, B.; Nadakatti, S. M. In *Physical Properties of Polymers Handbook*; Mark, J. E., Ed.; AIP Press: Woodbury, 1996.
(14) Zimmerman, C. M.; Singh, A.; Koros, W. J. *J. Polym. Sci., Part B: Polym. Phys.* **1998**, *36*, 1747−1755.
(15) Crank, J. *The Mathematics of Diffusion*, 2nd ed.; Oxford University Press: Oxford, 1975.
(16) Wang, R.; Cao, C.; Chung, T. *J. Membr. Sci.* **2002**, *198*, 259−271.
(17) Smit, E.; Mulder, M. H. V.; Smolders, C. A.; Karrenbeld, H.; van Eerden, J.; Feil, D. *J. Membr. Sci.* **1992**, *73*, 247−257.
(18) Zhang, R.; Mattice, W. L. *J. Membr. Sci.* **1995**, *108*, 15−23.
(19) Hofmann, D.; Ulbrich, J.; Fritsch, D.; Paul, D. *Polymer* **1996**, *37*, 4773−4785.
(20) Fried, J. R.; Sadad-Akhavi, M.; Mark, J. E. *J. Membr. Sci.* **1998**, *149*, 115−126.
(21) Bharadwaj, R. K.; Boyd, R. H. *Polymer* **1999**, *40*, 4229−4236.
(22) Cuthbert, T. R.; Wagner, N. J.; Paulitis, M. E.; Murgia, G.; D'Aguanno, B. *Macromolecules* **1999**, *32*, 5017−5028.
(23) Rallabandi, P. S.; Thompson, A. P.; Ford, D. M. *Macromolecules* **2000**, *33*, 3142−3152.
(24) Fritsch, D.; K. V. Peinemann, K. V. *J. Membr. Sci.* **1995**, *99*, 29−38.
(25) Neyertz, S.; Brown, D. *J. Chem. Phys.* **2001**, *115*, 708−717.
(26) Neyertz, S.; Brown, D.; Douanne, A.; Bas, C.; Albérola, N. D. *J. Phys. Chem. B* **2002**, *106*, 4617−4631.
(27) Pinel, E.; Brown, D.; Bas, C.; Mercier, R.; Albérola, N. D.; Neyertz, S. *Macromolecules* **2002**, *35*, 10198−10209.
(28) Liang, T.; Yang X.; Zhang, X. *J. Polym. Sci., Part B: Polym. Phys.* **2001**, *39*, 2243−2251.
(29) Lin, W.-H.; Chung, T.-S. *J. Membr. Sci.* **2001**, *186*, 183−193.
(30) Shimazu, A.; Miyazaki, T.; Matsushita, T.; Maeda, M.; Ikeda, K. *J. Polym. Sci., Part B: Polym. Phys.* **1999**, *37*, 2941−2949.
(31) Tsuzumi, H.; Toi, K.; Ito, T.; Kasai, T. *J. Appl. Polym. Sci.* **1997**, *64*, 389−397.
(32) Langsam, M.; Burgoyne, W. F. *J. Polym. Sci., Part A: Polym. Chem.* **1993**, *31*, 909−921.
(33) Coleman, M. R.; Koros, W. J. *J. Membr. Sci.* **1990**, *50*, 285−297.
(34) Mikawa, M.; Nagoaka S.; Kawakami, H. *J. Membr. Sci.* **1999**, *163*, 167−176.
(35) Matsumoto, K.; Xu, P.; Nishikimi, T. *J. Membr. Sci.* **1993**, *81*, 15−22.

(36) Matsumoto, K.; Xu, P. *J. Appl. Polym. Sci.* **1993**, *47*, 1961−1972.
(37) Stern, S. A.; Mi, Y.; Yamamoto, H.; St. Clair, A. K. *J. Polym. Sci., Part B: Polym. Phys.* **1989**, *27*, 1887−1906.
(38) Li, Y.; Wang, X.; Ding, M.; Xu, J. *J. Appl. Polym. Sci.* **1996**, *61*, 741−748.
(39) Xu, Z.-K.; Böhning, M.; Springer, J.; Glatz, F. P.; Mülhaupt, R. *J. Polym. Sci., Part B: Polym. Phys.* **1997**, *35*, 1855−1868.
(40) Kawakami, H.; Anzai, J.; Nagaoka, S. *J. Appl. Polym. Sci.* **1995**, *57*, 789−795.
(41) Kawakami, H.; Nakajima, K.; Nagaoka, S. *J. Membr. Sci.* **2003**, *211*, 291−298.
(42) As unit for the permeability coefficient *P* the Barrer is used; 1 Barrer = 10^{-10} cm^3(STP) cm/cm^2 s cm(Hg) where cm^3(STP) is the amount of gas in cm^3 at standard temperature and pressure (273 K, 1 bar). In SI units, 1 Barrer = 7.5×10^{-18} m^2/s Pa.
(43) Hayes, R. A. U.S. Patent 4,705,540, 1987.
(44) Wang. R.; Cao, Y.; Vora, R.; Tucker, J. R. *J. Appl. Polym. Sci.* **2001**, *82*, 2166−2173.
(45) Al-Masri, M.; Kricheldorf, H. R.; Fritsch D. *Macromolecules* **1999**, *32*, 7853−7858.
(46) Mikawa, M.; Nagaoka, S.; Kawakami, H. *J. Membr. Sci.* **2002**, *208*, 405−414.
(47) Xu, Z.; Xiao, L.; Wang, J.; Springer, J. *J. Membr. Sci.* **2002**, *202*, 27−34.
(48) Polymer User Guide, Amorphous Cell Section, Version 4.0.0; Molecular Simulations: San Diego, 1996.
(49) Sun, H.; Rigby, D. *Spectrochim. Acta* **1997**, *53A*, 1301−1323.
(50) Rigby, D.; Sun, H.; Eichinger, B. E. *Polym. Int.* **1997**, *44*, 311−330.
(51) Theodorou, D. N.; Suter, U. W. *Macromolecules* **1985**, *18*, 1467−1478; **1986**, *19*, 139−154.
(52) Hofmann, D.; Heuchel, M.; Yampolskii, Yu.; Khotimskii, V.; Shantarovich, V. *Macromolecules* **2002**, *35*, 2129−2140.
(53) Tocci, E.; Hofmann, D.; Paul, D.; Russo, N.; Drioli, E. *Polymer* **2001**, *42*, 521−533.
(54) Gusev, A. A.; Suter, U. W. *Phys. Rev. A* **1991**, *43*, 6488−6494.
(55) Gusev, A. A.; Arizzi, S.; Suter, U. W. *J. Chem. Phys.* **1993**, *99*, 2221−2227.
(56) Gusev, A. A.; Suter, U. W. *J. Chem. Phys.* **1993**, *99*, 2228−2234.
(57) Implemented as *gsnet*/*gsdiff* in InsightII/Discover software (Accelrys, Inc.).
(58) Heuchel, M.; Hofmann, D. *Desalination* **2002**, *144*, 67−72.
(59) Tanaka, K.; Okano, M.; Toshino, H.; Kita, H.; Okamoto, K. *J. Polym. Sci., Part B: Polym. Phys.* **1992**, *30*, 907−914.
(60) Yeom, C. K.; Lee, J. M.; Hong, Y. T.; Choi, K. Y.; Kim, S. C. *J. Membr. Sci.* **2000**, *166*, 71−83.
(61) This is done in the methodological developments of a current EU project PERMOD.
(62) Matsui, S.; Sato, H.; Nakagawa, T. *J. Membr. Sci.* **1998**, *141*, 31−43.
(63) This problem was analyzed by Accelrys. The error is removed in the actual version of the Compass force field.
(64) Nagai, K.; Toy, L. G.; Freeman, B. D.; Teraguchi, M.; Masuda, T.; Pinnau, I. *J. Polym. Sci., Part B: Polym. Phys.* **2000**, *38*, 1474−1484.
(65) Coleman, M. R.; Koros, W. J. *Macromolecules* **1997**, *30*, 6899−6905.
(66) Personal note: Dr. Fritsch (GKSS).
(67) *Positron and Positronium Chemistry*; Shrader, D. M., Jean, Y. C., Eds.; Elsevier: Amsterdam, 1988.
(68) Victor, J. G.; Torkelson, J. M. *Macromolecules* **1987**, *20*, 2241−2250.
(69) Bondar, V. I.; Freeman, B. D.; Yampolskii, Yu. P. *Macromolecules* **1999**, *32*, 6163−6171.
(70) Fujita, H. *Forschr. Hochpolym. Forsch.* **1961**, *3*, 1−47.
(71) Lee, W. M. *Polym. Eng. Sci.* **1980**, *20*, 65−69.
(72) Alentiev, A. Yu.; Yampolskii, Yu. P. *J. Membr. Sci.* **2002**, *206*, 291−306.
(73) Wilks, B. R.; Chung, W. J.; Rezac, M. E.; Meakin, P.; Hill, A. J. *Mater. Res. Soc. Symp. Proc.* **2003**, *752*, AA7.3.1−AA7.3.6.; *J. Polym. Sci., Part B: Polym. Phys.* **2003**, *41*, 2185−2199.
(74) Tanaka, K.; Kawai, T.; Kita, H.; Okamoto, K.; Ito, Y. *Macromolecules* **2000**, *33*, 5513−5517.
(75) Coleman, M. R.; Koros, W. J. *J. Polym. Sci., Part B: Polym. Phys.* **1994**, *32*, 1915−1926.

MA035360W